Electron-Hole Diffusion Lengths Exceeding 1 Micrometer in an Organometal Trihalide Perovskite Absorber

Samuel D. Stranks,[1] Giles E. Eperon,[1] Giulia Grancini,[2] Christopher Menelaou,[1] Marcelo J. P. Alcocer,[2] Tomas Leijtens,[1] Laura M. Herz,[1] Annamaria Petrozza,[2] Henry J. Snaith[1]*

Organic-inorganic perovskites have shown promise as high-performance absorbers in solar cells, first as a coating on a mesoporous metal oxide scaffold and more recently as a solid layer in planar heterojunction architectures. Here, we report transient absorption and photoluminescence-quenching measurements to determine the electron-hole diffusion lengths, diffusion constants, and lifetimes in mixed halide ($CH_3NH_3PbI_{3-x}Cl_x$) and triiodide ($CH_3NH_3PbI_3$) perovskite absorbers. We found that the diffusion lengths are greater than 1 micrometer in the mixed halide perovskite, which is an order of magnitude greater than the absorption depth. In contrast, the triiodide absorber has electron-hole diffusion lengths of ~100 nanometers. These results justify the high efficiency of planar heterojunction perovskite solar cells and identify a critical parameter to optimize for future perovskite absorber development.

Photovoltaic (PV) solar energy conversion has the potential to play a major role in future electricity generation. Most currently installed PV arrays consist of crystalline or polycrystalline silicon; in second generation thin-film architectures, light is absorbed and charge generated in a solid layer of this semiconductor (*1*). Beyond these existing technologies are a myriad of other emerging device concepts based on a broad range of materials, all vying to become the cheapest yet suitably efficient technology to enable widespread uptake of solar energy (*2*–*6*). Some of the most promising technologies for ultimate low-cost manufacture are solution-processed, such as organic photovoltaics (OPV), dye-sensitized solar cells (DSSCs), and semiconductor-sensitized or extremely thin absorber solar cells (*7*, *8*). However, these designs typically require a complex distributed donor-acceptor heterojunction to ionize charge because the exciton and charge carrier diffusion lengths in these materials are much shorter than the absorption depth (*7*, *9*–*11*). Emerging from the field of DSSCs, the inorganic-organic perovskite family of materials taking the form ABX_3 (A = $CH_3NH_3^+$; B = Pb^{2+}; and X = Cl^-, I^-, and/or Br^-) has within the past 12 months been used to fabricate high-performance hybrid solar cells, with reported power conversion efficiencies (η) of between 7 and 15% (*12*–*20*). These perovskite absorbers can be solution-processed in air and absorb light broadly across the solar spectrum. In the first experiments, the perovskite absorber was used as a sensitizer on mesoporous titania electrodes, along with a solid-state organic hole transporter (HTM) such as 2′-7,7′-tetrakis(*N*,*N*-di-*p*-methoxyphenylamine)-9,9 -spirobifluorene (spiro-OMeTAD), with the perovskite effectively replacing the dye conventionally used in a DSSC (*12*, *13*, *21*). Subsequently, the mixed halide $CH_3NH_3PbI_{3-x}Cl_x$ perovskite devices have been reported to yield η >12% when the titania is replaced with an insulating mesoporous alumina scaffold in meso-superstructured solar cells (MSSCs), demonstrating that the perovskite itself can at least sustain sufficient electron transport to enable highly efficient charge collection (*12*, *16*). Entirely removing the mesoporous alumina to create a thin-film planar heterojunction has resulted in solution-processed devices with close to 100% internal quantum efficiency for charge collection, but with lower η of 5% (*16*). Very recently, we have demonstrated that if an extremely uniform solid perovskite absorber film can be prepared—for example, through vapor deposition—then the highest efficiencies can be achieved in solid thin-film planar heterojunction architectures (*19*).

Despite the rapid increase in efficiency associated with the evolution of this technology, most of the fundamental questions concerning the photophysics and device operation remain unanswered. Arguably, the most critical question concerning whether mesostructured or planar heterojunction perovskite solar cells will eventually dominate is what the exciton or the electron and hole diffusion lengths are in these materials. We performed photoluminescence (PL)–quenching measurements in order to extract the electron-hole diffusion lengths in triiodide ($CH_3NH_3PbI_3$) and mixed halide ($CH_3NH_3PbI_{3-x}Cl_x$) perovskite thin films. We show that both electron and hole diffusion lengths are >1 μm for the mixed halide perovskite—a factor of ~5 to 10 greater than the absorption depth. In contrast, the diffusion lengths in the triiodide perovskite are only on the order of or slightly shorter than the absorption depth (~100 nm). The larger diffusion length in the mixed halide perovskite results from a much longer recombination lifetime and is consistent with far superior performance in MSSCs and planar heterojunction solar cells, as we demonstrate here.

PL quenching has been previously used successfully with organic semiconductors in order

[1]University of Oxford, Clarendon Laboratory, Parks Road, Oxford OX1 3PU, UK. [2]Center for Nano Science and Technology@PoliMi, Istituto Italiano di Tecnologia, Via Giovanni Pascoli 70/3, 20133, Milano, Italy.

*Corresponding author. E-mail: h.snaith1@physics.ox.ac.uk

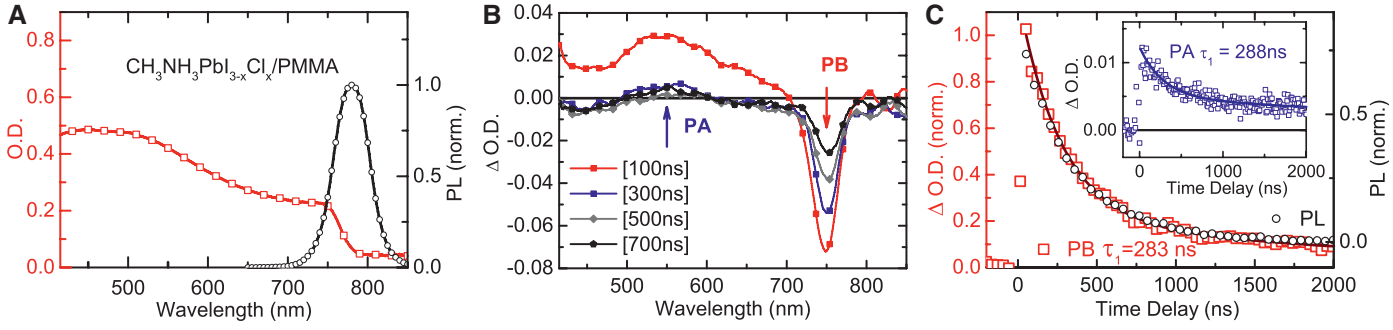

Fig. 1. Optical characterization of the mixed halide perovskite $CH_3NH_3PbI_{3-x}Cl_x$. (**A**) Absorption (red squares) and PL (black circles) spectra of a 270-nm-thick layer of $CH_3NH_3PbI_{3-x}Cl_x$ coated with PMMA. (**B**) Transient absorption spectra of $CH_3NH_3PbI_{3-x}Cl_x$ upon excitation at 500 nm (40 μJ/cm^2 pulses). Each gated spectrum has been integrated for 200 ns, and the PL was removed. (**C**) Normalized photobleaching (PB) (red squares, left axis) and PL dynamics (black circles, right axis) probed at 750 and 770 nm, respectively. Biexponential fitting of the PB data (dark red line) leads to a dominant time constant of τ_1 = 283 ± 6 ns, matching the dynamics of the PL (τ_e = 273 ± 7 ns), followed by a long-lived tail. (Inset) The photoinduced absorption (PA) dynamics at 550 nm (blue squares) with a biexponential fit (dark blue line; dominant time constant of τ_1 = 288 ± 12 ns), also matching the dynamics of the PL and the dominant component of the PB.

to determine the diffusion length of the photoexcited bound electron-hole pair, the exciton (*22*). By simply fabricating solid thin films in the presence or absence of an exciton-quenching layer, and modeling the PL decay to a diffusion equation, it is possible to accurately determine the exciton lifetime, diffusion rate, and diffusion length (*22*). However, for the organolead trihalide perovskites studied here, there is relatively little literature on probing the fundamental photophysics, and even the most basic question of whether PL occurs via free carrier recombination from the conduction and valence band electrons, or is preceded by exciton formation, remains unknown. Exciton binding energies for $CH_3NH_3PbI_3$ have been reported in the range of 37 to 50 meV in the orthorhombic phase (*23*–*25*). In principle, at ambient temperature these values are comparable to thermal energies (k_BT ~ 26 meV, where k_B is the Boltzmann constant and T is the temperature); thus, both free carriers and weakly bound excitons should coexist with interchange being possible between the two populations. However, provided all species (bound or free charges) decay with the same rate or through the same channel, the PL decay should still be representative of recombination or depopulation of electrons and holes from the perovskite film.

The $CH_3NH_3PbI_3$ and $CH_3NH_3PbI_{3-x}Cl_x$ perovskite precursor solutions were spin-coated on plasma-etched glass at room temperature in air, followed by annealing in air at 100°C for 45 min for the mixed halide and 150°C for 15 min for the triiodide (these temperatures and times correspond to the optimized conditions for best performance in the solar cells processed in air). Obtaining uniform and continuous perovskite films is essential for the subsequent PL-quenching measurements. As we have shown elsewhere, this is possible through precise control of processing conditions (*26*). In order to obtain air- and moisture-insensitive samples, the neat perovskite films (nonquenching samples) were sealed by spin-coating a layer of the insulating polymer poly(methylmethacrylate) (PMMA) on top. Full experimental details are given in the supplementary materials.

In Fig. 1A, we show the ultraviolet-visible absorption and PL spectra for a $CH_3NH_3PbI_{3-x}Cl_x$ thin film. The PL is right at the band edge, with very little Stokes-shift. This indicates little vibronic relaxation of the perovskite crystal, unlike organic semiconductors, which typically show large Stokes-shifts (*27*). The nanosecond–transient absorption (TA) spectra of a $CH_3NH_3PbI_{3-x}Cl_x$ film is shown in Fig. 1B. We observed a sharp negative band peaking at 750 nm together with a broad positive band at shorter wavelengths, peaking around 550 nm. We assign the negative band to the photobleaching (PB) of the band gap or exciton transition, whereas the positive band represents a photoinduced absorption (PA). From biexponential data fitting, we retrieved the dominant time constant of both the PB and PA to be ~280 ns, followed by a long-lived tail (>1 μs). As we show in Fig. 1C, the PA band decay (288 ± 12 ns) mirrors the PB recovery dynamics (283 ± 6 ns), suggesting that the spectra arise from the same population. If we compare the transient absorption decays with the transient PL decay (τ_e = 273 ± 7 ns, where τ_e is the time taken for the PL to fall to 1/*e* of its initial intensity), there is a strikingly close match. This indicates that the decay of the radiative species we are monitoring with the PL represents the decay of all absorbing species (free carriers or weakly bound excitons) in the perovskite film. We can therefore use PL-quenching measurements to determine a relevant diffusion constant and length in the perovskite films. We cannot, however, categorically determine whether this corresponds to the diffusion of free charge or excitons, but in either case, it will represent the relevant diffusion length for charge extraction in the solar cell. Additionally, we can safely exclude any contribution to the PL from trap states, which would be at lower energy and whose presence would otherwise complicate the subsequent PL-quenching analysis.

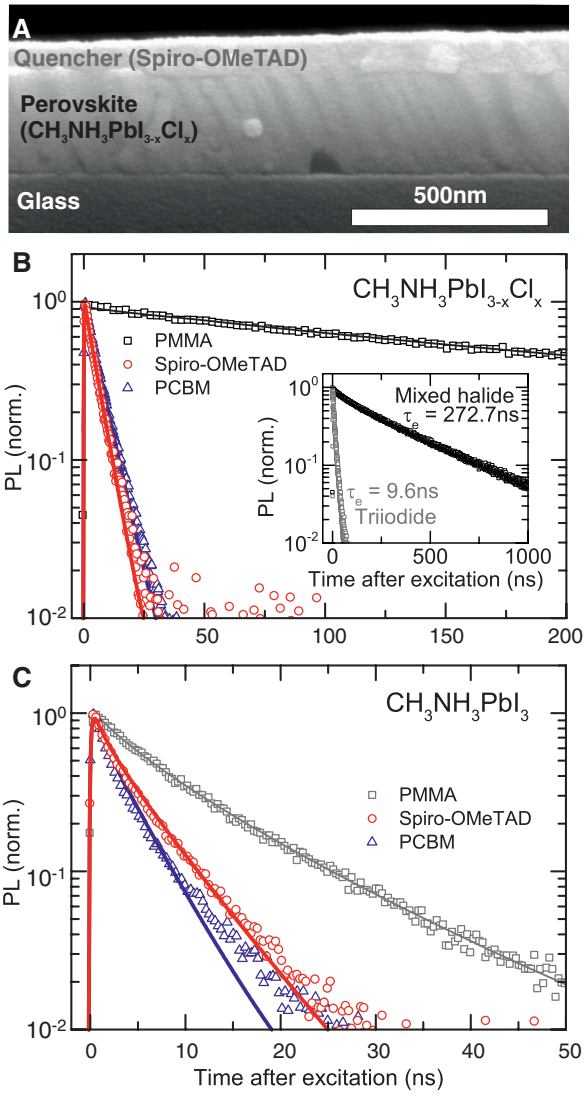

Fig. 2. PL measurements and fits to the diffusion model for the mixed halide and triiodide perovskites in the presence of quenchers. (**A**) Cross-sectional SEM image of a 270-nm-thick mixed halide absorber layer with a top hole-quenching layer of Spiro-OMeTAD. (**B** and **C**) Time-resolved PL measurements taken at the peak emission wavelength of the (B) mixed halide perovskite and (C) triiodide perovskite with an electron (PCBM; blue triangles) or hole (Spiro-OMeTAD; red circles) quencher layer, along with stretched exponential fits to the PMMA data (black squares) and fits to the quenching samples by using the diffusion model described in the text (details are available in the supplementary materials). A pulsed (0.3 to 10 MHz) excitation source at 507 nm with a fluence of 30 nJ/cm^2 impinged on the glass substrate side. (Inset) Comparison of the PL decay of the two perovskites (with PMMA) on a longer time scale, with lifetimes τ_e quoted as the time taken to reach 1/*e* of the initial intensity.

Table 1. Values for diffusion constants (D) and diffusion lengths (L_D) from fits to PL decays using the diffusion model described in the text. The errors quoted predominantly arise from perovskite film thickness variations, which are ± 35 nm for the triiodide perovskite films and ± 40 nm for the mixed halide perovskite films.

Perovskite	Species	D (cm^2 s^{-1})	L_D (nm)
$CH_3NH_3PbI_{3-x}Cl_x$	Electrons	0.042 ± 0.016	1069 ± 204
	Holes	0.054 ± 0.022	1213 ± 243
$CH_3NH_3PbI_3$	Electrons	0.017 ± 0.011	129 ± 41
	Holes	0.011 ± 0.007	105 ± 32

The quenching samples were prepared by means of spin-coating layers of either a hole-acceptor (Spiro-OMeTAD) or an electron-accepting fullerene [phenyl-C_{61}-butyric acid methyl ester (PCBM)] on top of the perovskite films. In Fig. 2A, we show a scanning electron microscopy (SEM) image of a ~270-nm-thick $CH_3NH_3PbI_{3-x}Cl_x$ absorber layer with a ~100-nm-thick Spiro-OMeTAD hole-quenching layer. We show SEM images of all sample configurations in figs. S1 and S2 and absorption spectra in fig. S3, which indicate that the mixed halide and triiodide perovskites have very similar bandgaps.

We present the time-resolved PL decays, measuring the peak emission at ~770 nm, for the mixed halide and triiodide perovskite absorbers in Fig. 2, B and C, respectively. The excitation fluence was kept to 0.03 μJ cm^{-2}/pulse so as to ensure that nonlinear effects, such as exciton-charge annihilation, are unlikely to occur. The thickness of the $CH_3NH_3PbI_{3-x}Cl_x$ films was 270 ± 40 nm, and the thickness of the $CH_3NH_3PbI_3$ films was 180 ± 35 nm, which is comparable with optimum device thicknesses. The corresponding steady-state spectra are shown in fig. S4. The PL decay of the neat $CH_3NH_3PbI_{3-x}Cl_x$ film exhibits a time-constant of τ_e = 273 ± 7 ns. The addition of the PCBM and Spiro-OMeTAD electron and hole-quenching layers accelerates the PL decay, with observed time constants τ_e of 6.1 ± 0.1 ns and 5.1 ± 0.1 ns, respectively. In contrast, the lifetime for the neat $CH_3NH_3PbI_3$ film is only τ_e = 9.6 ± 0.3 ns, and this is quenched further, but not by such a large fraction, to 3.17 ± 0.03 ns for electrons and 4.2 ± 0.1 ns for holes.

The PL decay dynamics were modeled by calculating the number and distribution of excitations in the film $n(x,t)$ according to the one-dimensional diffusion equation

$$\frac{\partial n(x,t)}{\partial t} = D\frac{\partial^2 n(x,t)}{\partial x^2} - k(t)n(x,t) \quad (1)$$

where D is the diffusion coefficient and $k(t)$ is the PL decay rate in the absence of any quencher material (further details are available in the supplementary materials) (*22*). The total decay rate k was determined by fitting a stretched exponential decay to the PL data measured from perovskite layers with PMMA. The effect of the quencher-layer was included by assuming that all photogenerated carriers that reach the interface are quenched, giving the boundary condition $n(L,t) = 0$, where $x = 0$ at the glass/perovskite interface and L is the perovskite film thickness. Because the samples were photo-excited from the glass substrate side of the samples, the initial distribution of photoexcitations was given by $n(x,0) = n_0 exp(-\alpha x)$, where α is the absorption coefficient. The average diffusion length L_D of the species was then determined from $L_D = \sqrt{D\tau_e}$, where τ_e is the recombination lifetime in the absence of a quencher. If free charges are predominantly created upon photoexcitation, the PL decay represents the depopulation of charge carriers, and we estimated the diffusion coefficients for holes or electrons depending on which quenching layer is used. The results from the diffusion model fits are shown in Fig. 2, B and C, and the parameters summarized in Table 1. The diffusion lengths for both electrons and holes in the mixed halide perovskite are greater than 1 μm, which is much longer than the absorption depth of 100 to 200 nm. This indicates that there should be no requirement for meso- or nanostructure with this specific perovskite absorber. In contrast, the triiodide perovskite $CH_3NH_3PbI_3$ films have over one order of magnitude shorter diffusion length of ~100 nm for both electrons and holes, which is too short with respect to the absorption depth for this material to perform at the highest efficiencies in the thin-film configuration. The close similarity of the derived electron and hole diffusion coefficients and lengths in each of these perovskites either indicates very similar mobility for both electrons and holes, or it indicates that the predominant diffusion species is the weakly bound exciton. We can unfortunately not discriminate between the two from these results.

To confirm the importance of the determined diffusion length in full solar cells, and to test whether the measurement correlates well with device results, we fabricated solution-processed thin-film planar heterojunction solar cells with both the mixed halide and triiodide perovskites. We formed solid perovskite films on fluorine-doped tin oxide (FTO)–coated glass substrates, coated with an n-type TiO_2 compact layer so as to ensure selective collection of electrons at the FTO substrate. Subsequently, p-type spiro-OMeTAD was deposited as a hole-transporting layer so as to form a planar p-i-n heterojunction architecture. Current-voltage characteristics for the best devices fabricated are shown in Fig. 3. The $CH_3NH_3Pb\ I_{3-x}Cl_x$ planar heterojunction solar cells reach power conversion efficiencies in excess of 12%, which is the highest solution-processed planar heterojunction perovskite efficiency reported to date. In contrast, we were only able to attain η of ~4% with the $CH_3NH_3PbI_3$. Upon optimization of devices to obtain the highest efficiencies, we found that a thick layer of $CH_3NH_3Pb\ I_{3-x}Cl_x$ was preferable (~500 nm). However, the best $CH_3NH_3PbI_3$ cells had a perovskite layer thickness of only 140 nm. This observation is consistent with the diffusion-length calculations, in which the triiodide films are limited by the ~100-nm diffusion length, so that photogenerated charge in thicker films cannot be efficiently extracted before recombining. A full set of device results and average performances is given in table S1.

This work indicates that with correct tuning of the perovskite absorber, nano- or mesostructures are not necessary in order to achieve highly efficient charge generation and collection. Our results hence pave the way for further advances in planar heterojunction perovskite solar cells. Fundamentally, there still remain many open questions for the community concerning the nature of the excited state, the relative fraction of free and bound charge pairs at room temperature, and the interplay between the two species. Furthermore, this work introduces a new question as to why the small addition of chloride ions to the organolead triiodide perovskite results in such a striking increase in the electron-hole diffusion length, predominantly arising from a substantial inhibition of nonradiative electron-hole recombination. Understanding these subtleties will enable further improvement of the current family of materials.

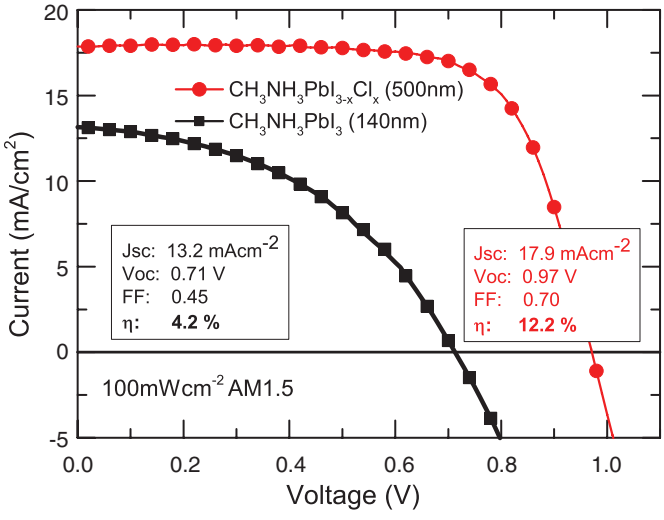

Fig. 3. Current-voltage curves for optimized planar heterojunction perovskite solar cells. $CH_3NH_3PbI_{3-x}Cl_x$ (red line, circle symbols) and $CH_3NH_3PbI_3$ (black line, square symbols) cells were both measured under 100 mW cm^{-2} AM1.5 simulated sunlight. J_{SC} is the short-circuit current, V_{OC} is the open-circuit voltage, FF is the fill factor, and η is the power conversion efficiency.

References and Notes

1. S. Chu, A. Majumdar, *Nature* **488**, 294–303 (2012).
2. B. O'Regan, M. Gratzel, *Nature* **353**, 737–740 (1991).
3. Z. He *et al.*, *Nat. Photonics* **6**, 593 (2012).
4. R. A. J. Janssen, J. Nelson, *Adv. Mater.* **25**, 1847–1858 (2013).
5. T. Todorov, D. B. Mitzi, *Eur. J. Inorg. Chem.* **2010**, 17–28 (2010).
6. E. H. Sargent, *Nat. Photonics* **6**, 133–135 (2012).
7. M. Graetzel, R. A. J. Janssen, D. B. Mitzi, E. H. Sargent, *Nature* **488**, 304–312 (2012).
8. G. Hodes, D. Cahen, *Acc. Chem. Res.* **45**, 705–713 (2012).
9. G. Yu, J. Gao, J. C. Hummelen, F. Wudl, A. J. Heeger, *Science* **270**, 1789–1791 (1995).

10. O. V. Mikhnenko *et al.*, *Energy Environ. Sci.* **5**, 6960 (2012).
11. J. J. M. Halls *et al.*, *Nature* **376**, 498–500 (1995).
12. M. M. Lee, J. Teuscher, T. Miyasaka, T. N. Murakami, H. J. Snaith, *Science* **338**, 643–647 (2012).
13. H.-S. Kim *et al.*, *Sci. Rep.* **2**, 591 (2012).
14. J. H. Heo *et al.*, *Nat. Photonics* **7**, 486 (2013).
15. J. H. Noh, S. H. Im, J. H. Heo, T. N. Mandal, S. I. Seok, *Nano Lett.* **13**, 1764–1769 (2013).
16. J. M. Ball, M. M. Lee, A. Hey, H. J. Snaith, *Energy Environ. Sci.* **6**, 1739 (2013).
17. J. Burschka *et al.*, *Nature* **499**, 316–319 (2013).
18. A. Abrusci *et al.*, *Nano Lett.* **13**, 3124–3128 (2013).
19. M. Liu, M. B. Johnston, H. J. Snaith, *Nature* **501**, 395–398 (2013).
20. W. Zhang *et al.*, *Nano Lett.* **13**, 4505–4510 (2013).
21. A. Kojima, K. Teshima, Y. Shirai, T. Miyasaka, *J. Am. Chem. Soc.* **131**, 6050–6051 (2009).
22. P. E. Shaw, A. Ruseckas, I. D. W. Samuel, *Adv. Mater.* **20**, 3516–3520 (2008).
23. T. Ishihara, *J. Lumin.* **60-61**, 269–274 (1994).
24. K. Tanaka *et al.*, *Solid State Commun.* **127**, 619–623 (2003).
25. M. Hirasawa, T. Ishihara, T. Goto, K. Uchida, N. Miura, *Physica B* **201**, 427–430 (1994).
26. G. E. Eperon, V. M. Burlakov, P. Docampo, A. Goriely, H. J. Snaith, *Advanced Funtional Materials*, published online 9 September 2013 (10.1002/adfm.201302090).
27. J. R. Lakowicz, *Principles of Fluorescence Spectroscopy* (Springer London, Limited, 2007).

Acknowledgments: This project was funded by the Engineering and Physical Sciences Research Council, the European Research Council (ERC-StG 2011 HYPER project 279881), Oxford Photovoltaics through a Nanotechnology KTN CASE award, and by a Royal Society Wolfson exchange grant. The authors thank V. D'Innocenzo for technical support and J. Alexander-Webber for atomic force microscopy supporting measurements. A.P. and H.J.S. thank "The Royal Society International Exchanges Scheme 2012/R2." S.D.S. thanks Worcester College, Oxford, for additional financial support. Solar cells based on the perovskite materials studied in this report are being commercialized by Oxford Photovoltaics, a spin-out company from the University of Oxford.

Supplementary Materials

www.sciencemag.org/content/342/6156/341/suppl/DC1
Materials and Methods
Figs. S1 to S4
Tables S1 to S3

30 July 2013; accepted 4 September 2013
10.1126/science.1243982

Long-Range Balanced Electron- and Hole-Transport Lengths in Organic-Inorganic $CH_3NH_3PbI_3$

Guichuan Xing,[1]* Nripan Mathews,[2,3,4]*† Shuangyong Sun,[2] Swee Sien Lim,[1] Yeng Ming Lam,[2,5] Michael Grätzel,[3,6] Subodh Mhaisalkar,[2,3] Tze Chien Sum[1]†

Low-temperature solution-processed photovoltaics suffer from low efficiencies because of poor exciton or electron-hole diffusion lengths (typically about 10 nanometers). Recent reports of highly efficient $CH_3NH_3PbI_3$-based solar cells in a broad range of configurations raise a compelling case for understanding the fundamental photophysical mechanisms in these materials. By applying femtosecond transient optical spectroscopy to bilayers that interface this perovskite with either selective-electron or selective-hole extraction materials, we have uncovered concrete evidence of balanced long-range electron-hole diffusion lengths of at least 100 nanometers in solution-processed $CH_3NH_3PbI_3$. The high photoconversion efficiencies of these systems stem from the comparable optical absorption length and charge-carrier diffusion lengths, transcending the traditional constraints of solution-processed semiconductors.

An ideal solar cell material should combine good optical absorption characteristics with efficient charge-transport properties. Low-temperature solution-processed light-harvesting films prepared by techniques such as spin-coating and chemical bath deposition are typically amorphous or poorly crystalline (*1*–*3*), consequently suffering from poor charge-carrier transport (*4*). This limitation necessitates device designs that decouple light absorption and charge-carrier transport lengths, including light-trapping strategies such as plasmonics (*5*, *6*) as well as the sensitized solar cell architecture (*7*, *8*). The recent development of organic-inorganic halide perovskite materials such as $CH_3NH_3PbI_3$ as light harvesters in solid-state sensitized solar cells has led to reports of impressive efficiency values of up to 15% (*9*). This remarkable material has been used in a variety of photovoltaic architectures. A configuration used by Kim *et al.* (*10*) and Heo *et al.* (*11*) sandwiches the thin perovskite layer between a rough mesoporous TiO_2 photoanode and a hole-transporting layer such as 2,2′,7,7′-tetrakis(*N*,*N*-di-*p*-methoxyphenylamino)-9,9′-spirobifluorene (Spiro-OMeTAD). Lee *et al.* (*12*) have shown that efficient solar cells can be fabricated by replacing the TiO_2 photoanode with an insulating Al_2O_3 scaffold, implying good electron-transport properties. Unexpectedly, Etgar *et al.* (*13*) reported an efficiency of 5.5% in a configuration without the hole-transporting layer, indicating good hole-transport properties. These indications of ambipolar charge-transport capabilities are supported by a recent report by Ball *et al.* (*14*) that demonstrated that ~350-nm-thick planar films sandwiched between a TiO_2 compact layer and a hole-transporting layer can generate short-circuit current densities of 15 mA/cm^2. These reports together imply that the electron- and hole-transport lengths within these organic-inorganic hybrid materials are high. Nonetheless, the innate dynamics of the photoexcited electrons and holes in $CH_3NH_3PbI_3$ driving the high efficiencies in these solar cells are unknown. Herein, through femtosecond transient optical spectroscopy of $CH_3NH_3PbI_3$ heterojunctions with selective electron and hole extraction, we successfully decoupled electron and hole dynamics and show evidence of long electron- and hole-transport lengths (both over 100 nm). Our findings indicate that this class of materials does not suffer from the bottleneck of low collection lengths that handicap typical low-temperature solution-processed photovoltaic materials.

In this study, electron-extraction layers {such as [6,6]-phenyl-C_{61}-butyric acid methyl ester (PCBM), C_{60}} with conduction band levels below that of $CH_3NH_3PbI_3$ and hole-extraction layers [such as Spiro-OMeTAD, poly(3,4-ethylenedioxythiophene) poly(styrenesulfonate) (PEDOT:PSS)] with valence band levels above $CH_3NH_3PbI_3$ were interfaced to $CH_3NH_3PbI_3$ to permit decoupling of the electron and hole dynamics (fig. S1). Comparing measurements on bare $CH_3NH_3PbI_3$ against $CH_3NH_3PbI_3$/hole acceptor bilayers and $CH_3NH_3PbI_3$/electron acceptor bilayers enables identification of electron and hole signatures in the organic-inorganic halide. Under identical experimental conditions, the photoluminescence (PL) quantum yield of the 65-nm-thick $CH_3NH_3PbI_3$ is greatly reduced when the perovskite is interfaced with an electron-extracting PCBM layer or a hole-extracting Spiro-OMeTAD layer (Fig. 1A). The PL intensity is quenched by a factor of 12.5 in the bilayer with Spiro-OMeTAD and by a factor of 50 in the bilayer with PCBM (table S1). Given that the current configurations are ideal layered systems (figs. S2 and S3), these high degrees of PL quenching, comparable to closely blended donor-acceptor system, are particularly revealing (*15*–*19*). With a linear absorption coefficient of 5.7×10^4 cm^{-1} at 600 nm (Fig. 2A and fig. S4), near-homogenous generation of the charge carriers in these 65-nm $CH_3NH_3PbI_3$ layers can be ensured (*20*). The PL quenching is expected to originate from the charge-carrier extraction across the interface (*21*–*27*). Efficient PL quenching suggests that the charge-carrier diffusion length inside the $CH_3NH_3PbI_3$

[1]Division of Physics and Applied Physics, School of Physical and Mathematical Sciences, Nanyang Technological University (NTU), 21 Nanyang Link, 637371 Singapore. [2]School of Materials Science and Engineering, NTU, Nanyang Avenue, 639798 Singapore. [3]Energy Research Institute @NTU (ERI@N), Research Techno Plaza, X-Frontier Block, Level 5, 50 Nanyang Drive, 637553 Singapore. [4]Singapore-Berkeley Research Initiative for Sustainable Energy, 1 Create Way, 138602 Singapore. [5]Institute of Materials for Electronic Engineering II, Rheinisch Westfälische Technische Hochschule–Aachen, Sommerfeldstrasse 24, D-52074 Aachen, Germany. [6]Laboratory of Photonics and Interfaces, Department of Chemistry and Chemical Engineering, Swiss Federal Institute of Technology, Station 6, CH-1015 Lausanne, Switzerland.

*These authors contributed equally to this work.
†Corresponding author. E-mail: tzechien@ntu.edu.sg (T.C.S.); nripan@ntu.edu.sg (N.M.)

Science

Samuel D. Stranks, Giles E. Eperon, Giulia Grancini, Christopher Menelaou, Marcelo J. P. Alcocer, Tomas Leijtens, Laura M. Herz, Annamaria Petrozza and Henry J. Snaith

Science **342** (6156), 341-344.
DOI: 10.1126/science.1243982

Unrestricted Travel in Solar Cells

In the past 2 years, organolead halide perovskites have emerged as a promising class of light-harvesting media in experimental solar cells, but the physical basis for their efficiency has been unclear (see the Perspective by **Hodes**). Two studies now show, using a variety of time-resolved absorption and emission spectroscopic techniques, that these materials manifest relatively long diffusion paths for charge carriers energized by light absorption. **Xing *et al.*** (p. 344) independently assessed (negative) electron and (positive) hole diffusion lengths and found them well-matched to one another to the ~100-nanometer optical absorption depth. **Stranks *et al.*** (p. 341) uncovered a 10-fold greater diffusion length in a chloride-doped material, which correlates with the material's particularly efficient overall performance. Both studies highlight effective carrier diffusion as a fruitful parameter for further optimization.

Science (print ISSN 0036-8075; online ISSN 1095-9203) is published by the American Association for the Advancement of Science, 1200 New York Avenue NW, Washington, DC 20005.